metals

MDPI

Communication

High Manganese TWIP Steel with Increased Corrosion Resistance

Pavel Podany [1,*], Tomas Gregor [1], Tomas Studecky [2] and Crtomir Donik [3]

[1] Department of Materials Analysis, COMTES FHT a.s., Prumyslova 995, 334 41 Dobrany, Czech Republic
[2] Department of Metallurgical Technologies, COMTES FHT a.s., Prumyslova 995, 334 41 Dobrany, Czech Republic
[3] Department of Physics and Chemistry of Materials, IMT—Institute of Metals and Technology, Lepi Pot 11, 1000 Ljubljana, Slovenia
* Correspondence: pavel.podany@comtesfht.cz; Tel.: +420-377197340

Abstract: The paper describes the development of austenitic steel with the TWIP effect, which is alloyed with chromium to increase corrosion resistance. The experimental heat of this steel was cast in an experimental melting furnace and subsequently subjected to hot and cold rolling. After cold rolling, the appropriate recrystallization annealing temperature was applied to obtain the optimal austenitic grain size. X-ray diffraction proved that the steel contains a fully austenitic structure. After recrystallization annealing, the sheets achieved a TS of more than 950 MPa with an elongation of 40%. The corrosion resistance of this steel is increased with the addition of chromium.

Keywords: TWIP; cold/hot rolling; mechanical properties; corrosion

Citation: Podany, P.; Gregor, T.; Studecky, T.; Donik, C. High Manganese TWIP Steel with Increased Corrosion Resistance. *Metals* **2022**, *12*, 1765. https://doi.org/10.3390/met12101765

Academic Editor: Zhengyou Tang

Received: 18 August 2022
Accepted: 19 October 2022
Published: 20 October 2022

1. Introduction

Steel is still the most widely used material in the production of car bodies, and the continuous development of the automotive industry has created a demand for strong and ductile steels that must exhibit high strength and high ductility [1]. In frontal and rear impacts, high impact energy absorption is required if injury to occupants is to be avoided. In the case of a side impact or in the event of a rollover onto the roof, intrusion protection is also required [2]. Austenitic steels are widely used in many applications because they have an excellent strength-to-ductility ratio and good wear and corrosion resistance. High-manganese TWIP (Twinning Induced Plasticity) steels are highly ductile and high-strength Mn-austenitic steels are characterized by a high degree of strengthening due to the twinning mechanism, but at the same time retain the formability of deep-drawing steels [3]. They are very attractive for automotive applications because of their high energy absorption, which is up to twice that of conventional steels. High strength and high stiffness can improve safety. In addition, the possibility of using thinner sheets while maintaining sufficient strength can reduce vehicle weight and, consequently, lower fuel consumption [4].

The main alloying element in TWIP steels is manganese (Mn). The high manganese content (15 to 33%) ensures an austenitic phase. In addition, these steels tend to be alloyed with other elements such as silicon (Si), aluminium (Al), chromium (Cr) or nitrogen (N) to improve desirable properties [3]. As a result, they generally have very high ultimate strengths (even more than 1000 MPa) and high ductility values (up to 125%) [5,6].

There are very few research papers dealing with the topic of corrosion in TWIP steels. Generally, the corrosion resistance of standard TWIP steels is not good [7,8], and various efforts are being made to improve it by alloying with other elements such as chromium and aluminium, which should provide passivation and corrosion resistance. In corrosion-resistant TWIP steels, a protective layer is formed in corrosive environments. For example, in TWIP steel with a composition of Fe-30Mn-8Al-6Cr prepared by Hamada [9], the aluminium and chromium contribute to forming a passivation layer that protects the

material from the further development of corrosion attack. As a result, this steel resists nitric acid solutions very well. However, resistance in chlorine solutions was worse. In addition, the characterisation of 30Mn-4Al-4Cr steel and four steels with varying amounts of 25Mn-1-8 Al are found in his work.

In [10], the susceptibility of high manganese TWIP steel to stress corrosion cracking (SCC) in 3.5% NaCl solution was investigated using slow strain rate tests (SSRT), constant load (CL) and fractography. The steel composition was 26.34% Mn, 4.84% Al, 0.018% C, 0.065% Cr, 0.035% Ni, 0.284% Pb, 0.04% Nb, 0.013% N, 0.04% S. The strain rates used for SSRT were in the range of 10^{-6} to 10^{-8} s^{-1}. Samples tested in air revealed a ductile type of failure, while those tested in a corrosive solution showed brittleness attributed to corrosion cracking.

Three steels of composition 26% Mn, 2.8% Al, 0.33% C, 0.2% Si, 0.012% N with different Cr contents ranging from 1.1 to 4% Cr were prepared in [11]. The effects of chromium on the corrosion properties of this TWIP steel were studied. The results showed that Cr content distinctly affects high manganese TWIP steels' mechanical properties and brittleness. The steel sheets' yield and tensile strength improved with increasing Cr content, while the ductility decreased. The yield and tensile strength were enhanced by the increase of Cr content in the matrix, which caused a decrease in the average grain size and a larger amount of intergranular precipitated $Cr_{23}C_6$ phases. In addition, when the Cr content increased, the fracture mode changed from ductile fracture with coarse grooves and crack tip (Cr content $\leq$ 2.35%) to intergranular fracture (when Cr content is 3.95%). Furthermore, Cr content greatly affected the corrosion properties of high manganese TWIP steels. Increasing the Cr content increased the corrosion resistance of the annealed steel sheets. The proportion of low-angle boundary (LAB) decreased with increasing Cr content, thus increasing the corrosion resistance.

The corrosion behaviour of Fe-Mn-Al-Si steel subjected to cold forming (0%, 20%, and 35% was investigated in [12]. It was exposed to acidic (0.1 M H_2SO_4), alkaline (0.1 M NaOH) and chloride-containing (3.5% NaCl) environments using potentiodynamic polarization experiments. Interestingly, cold drawing did not change the corrosion sensitivity of TWIP steel in any of these environments. However, the steel exhibited the highest corrosion sensitivity in acidic environments and the lowest in alkaline environments. The scanning electron microscope analysis of samples of the corroded steel revealed a highly localized attack in the acidic environment and some degree of pitting corrosion in the chloride-containing solution.

In [13], TWIP steel with the composition Fe-25Mn-12Cr-0.3C-0.4N in was developed and fabricated. The resulting austenitic structure without δ-ferrite or ε-martensite was characterised. Tensile tests revealed a yield strength of 460 MPa and a tensile strength of 880 MPa. Electrochemical corrosion tests showed a good degree of passivation in 0.5 M H_2SO_4 electrolyte. The structure, mechanical properties and corrosion resistance are compared with conventional TWIP steels such as Fe-25Mn-3Al-3Si and Fe-22Mn-0.6C, which this alloy outperformed in terms of properties.

The main goal of the presented research was to develop a fully austenitic steel with a twinning mechanism during plastic deformation. In comparison to the results presented by the other studies mentioned above, the new steel should reach a higher tensile strength, above 900 MPa, and yield strength above 600 MPa together with good elongation. A further goal was to increase its corrosion resistance and achieve results similar to some grades of martensitic stainless steel.

2. Experiment Description

Chemical composition (see Table 1) was measured using the Bruker Q8 Magellan optical emission spectrometer (Bruker GmbH, Karlsruhe, Germany). The heats were melted and cast in a VIP vacuum induction furnace (PZSK, Kladno, Czech Republic) into a round ingot mould. After cooling, the ingots were further reheated in a furnace to a rolling temperature of 1100 °C. They were then hot-rolled on the experimental Rolling

Mill (PZSK, Kladno, Czech Republic) to strips with a thickness of 9 mm. The rolled strips were annealed at 950 °C for 2 h. After grinding, the annealed strips were cold rolled to a thickness of 2.5 mm with interoperation annealing at 950 °C. After cold rolling, the sheets were subjected to recrystallization annealing in a Schmetz vacuum furnace (IVA SCHMETZ GmbH, Menden, Germany) at 925 °C for 2 h with slow cooling. The main goal of this annealing was to induce recrystallization in the cold-rolled microstructure and thus increase the plasticity of the experimental steel. The X-ray diffraction (XRD) analysis for the phase analysis was carried out using a BRUKER D8 DISCOVER (Bruker GmbH, Karlsruhe, Germany). EBSD (Electron backscattered diffraction) analysis was done on a JEOL IT 500 HR (Jeol Ltd., Akishima, Japan) scanning electron microscope equipped with HIKARI super EBSD camera by EDAX™ (EDAX, LLC, Warrendale, PA, USA). Data analysis was carried out in the EDAX OIM Analysis software. Tensile tests were carried out on a Zwick/Roell 250 kN electromechanical testing machine (Zwick GmbH and Co. KG., Ulm, Germany). The deformation was measured using a strain gauge extensometer. Characteristic dimensions were measured before and after the test. Corrosion tests were performed on a Gamry PC4 electrochemical potentiostat (Gamry Instruments, Inc., Warminster, PA, USA).

Table 1. Chemical composition of the experimental steel.

Heat No.	C	Mn	Cr	Si	N	Mo	Fe
T19-161	0.33	27.5	12.9	0.14	0.54	1.1	Bal.

3. Results and Discussion

3.1. Microstructure

The X-ray diffraction (XRD) analysis for estimating the austenite volume fraction was carried out using a BRUKER D8 DISCOVER diffractometer with Cu Kα radiation (wavelength, λ = 0.15406 nm). This analysis proved the presence of a fully austenitic microstructure in both the cold rolled and annealed states with no presence of deformation induced α (alpha) or ε (epsilon) martensite (see Figure 1).

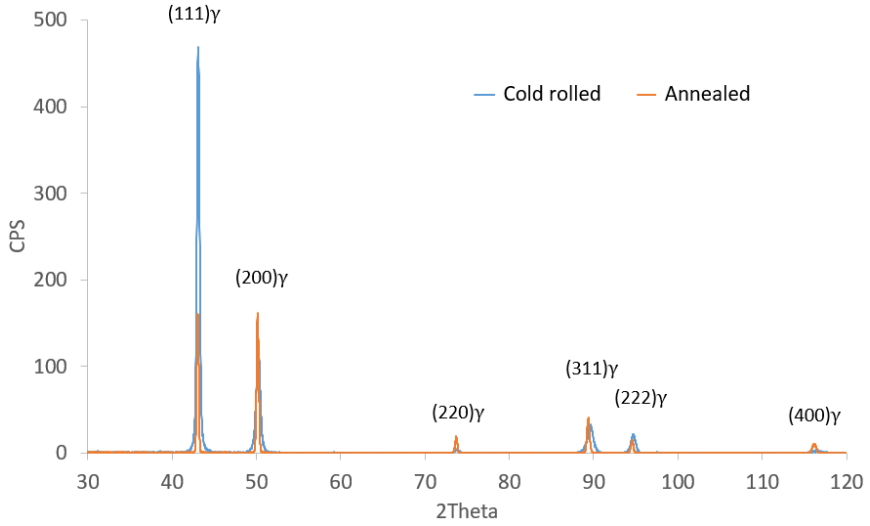

Figure 1. X-ray diffraction patterns of cold rolled and annealed samples of experimental steel.

The microstructure of the sheet after cold rolling and annealing was documented using a scanning electron microscope. Various etchants were used to try to develop the microstructure, but none succeeded in highlighting the grain boundaries well, and various unrelated artefacts were observed in the microstructure instead. In the end, documentation of as-polished samples using the low accelerating voltage of a scanning electron microscope, a low working distance and a sensitive backscattered electron detector proved to be the

best method. Under these conditions, individual austenitic grains are well distinguished. The fine-grained microstructure of equiaxed austenitic grains can thus be observed in the experimental steel (Figure 2). Fine globular chromium carbides are evenly distributed in the microstructure.

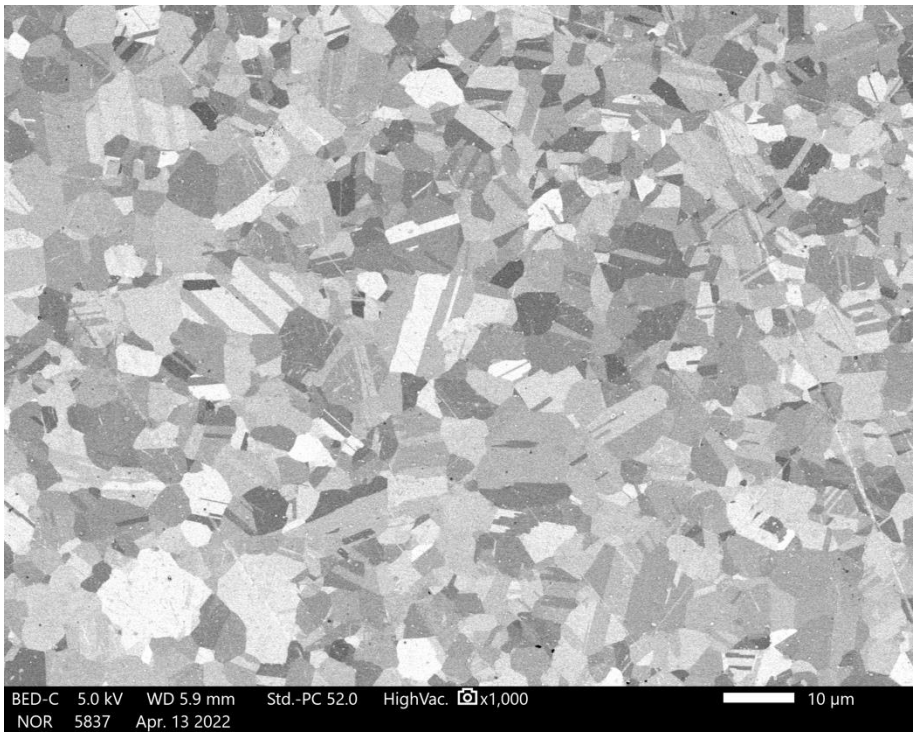

Figure 2. Back-scattered electron image of the microstructure.

The EBSD analysis of the microstructure was performed on two states of the microstructure. In the state after cold rolling at 50% reduction (from 5 to 2.5 mm)—Figure 3a) and in the state after annealing at 925 °C for two hours—Figure 3b. Recrystallization annealing after cold rolling promoted a substantial refinement of the microstructure. For the microstructure after cold rolling, the largest grain area fraction was G 4 (according to ASTM E112—Standard Test Methods for Determining Average Grain Size), Figure 3c. Annealing led to grain refinement with an average grain size G = 13.5 according to ASTM 112 (see Figure 3d).

Further EBSD analysis also demonstrated a twinning mechanism during plastic deformation. This is evident in Figure 4, where twin formation within the larger parent grains near the fracture area of the tensile test sample can be seen. In addition, the twin boundaries and thus newly formed twins are evident (marked by yellow arrows).

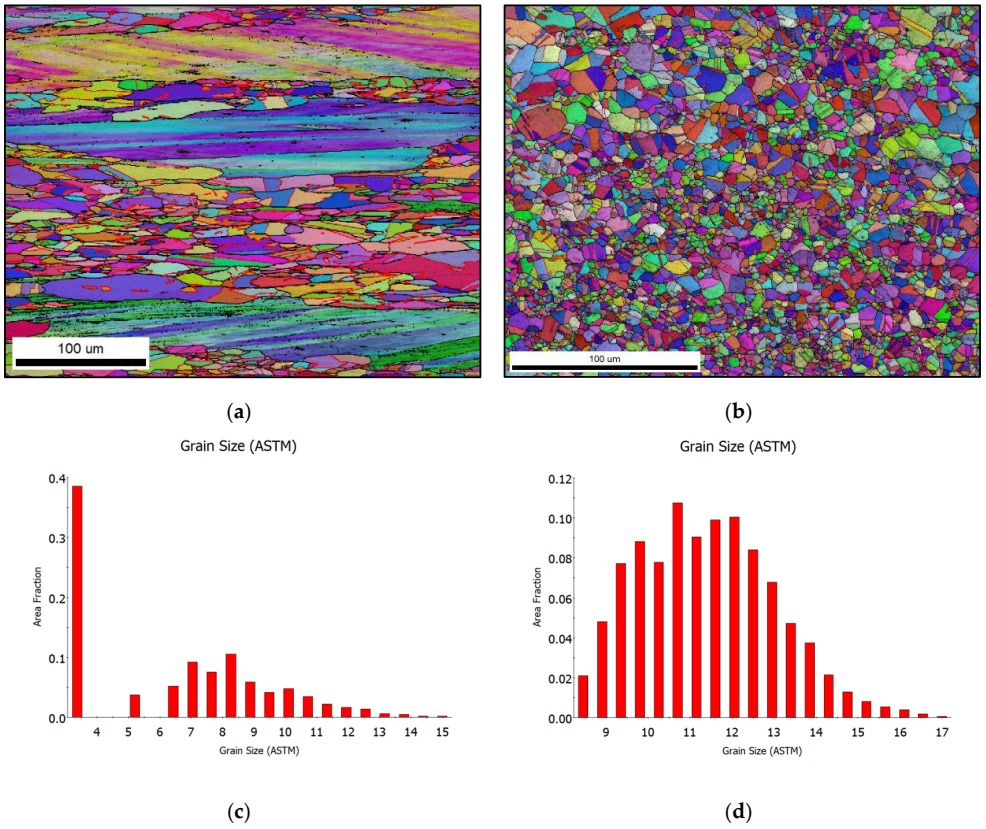

Figure 3. EBSD analysis—images (image quality map + inverse pole figures map, twin boundaries are red) and charts: (**a**) cold rolled state of experimental steel; (**b**) annealed state of experimental steel (925 °C/2 h); (**c**) grain size chart of cold rolled experimental steel; and (**d**) grain size chart of annealed experimental steel.

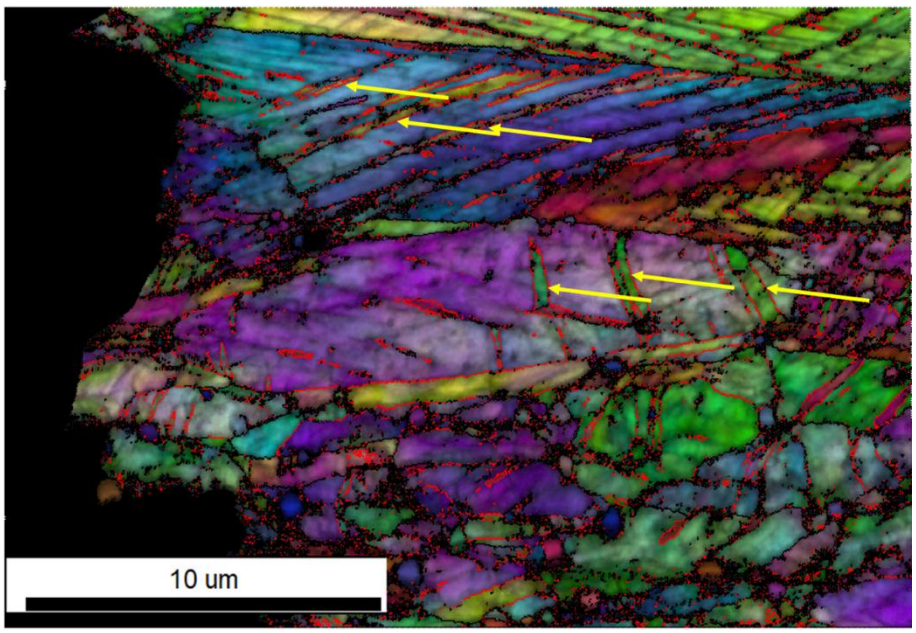

Figure 4. EBSD analysis of the sample microstructure after tensile test near the fracture area, grain boundaries with angles 55° to 65° are marked with red lines (boundaries of deformation twins).

3.2. Mechanical Properties

Tensile tests were carried out on a Zwick/Roell 250 kN electromechanical testing machine. Three flat samples were extracted from the annealed sheet (marked as T19-161_1, T19-161_2 and T19_161_3). The yield strength (YS), tensile strength (TS), elongation (El) and reduction of area (RA) are summarised in Table 2. Figure 5 shows engineering stress-strain curves. All the tested samples exhibit excellent combinations of high strength and ductility. Such results can be attributed mainly to the twinning mechanism introduced by alloying with a high manganese content and to the fine-grained microstructure resulting from a combination of cold rolling and recrystallisation annealing.

Table 2. Mechanical properties of experimental steel.

Heat No.	YS (0.2%) (MPa)	TS (MPa)	El (%)	RA (%)
T19-161	628.9 ± 5.3	976.7 ± 1.3	40.0 ± 0.5	48.4 ± 2.2

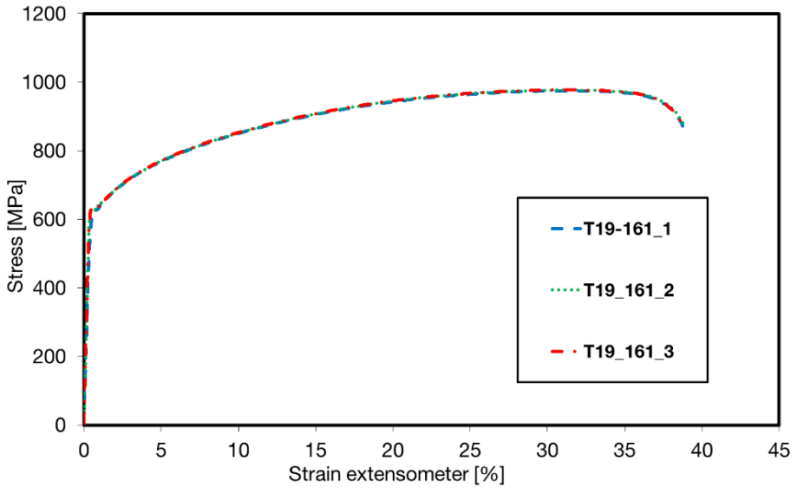

Figure 5. Engineering stress-strain curves of tensile test performed on experimental steel.

3.3. Corrosion Behaviour

The corrosion resistance of the experimental steel sample with a metallographically polished surface was verified in model seawater at 70 °C. The model seawater solution contained 3.5 wt.% NaCl. The Gamry PC4 electrochemical potentiostat measuring system was used for the measurements. The open circuit potential (E_{oc}) was stabilized for 3600 s. The polarization resistance was measured within ±0.02 V/E_{oc} at a scan rate of 0.125 mV/s. The cyclic polarization curve was measured in the range of −0.2 V/E_{oc} to 1.2 V/E_{oc} at a scan rate of 0.5 mV/s. A pressure cell was used for the measurements. A Pt counter electrode and a reference silver chloride electrode (ACLE) were used for all measurements. The polarization resistance (Rp), cyclic polarization curve (Cp) and corrosion potential (E_{corr}) of the supplied sample were measured. The resulting values are the average value of three measurements.

During the test, the surface layer barrier effect was well observed in the sample (Figure 6). The current density in the area of the barrier effect of the surface layer is approximately $i_{barrier}$ = 14.8 ± 6.2 μA.cm^{-2} (Figure 6, Table 3). The breakdown of the surface layer occurred at $E_{barrier}$ = −355 ± 9 (Figure 6, Table 3).

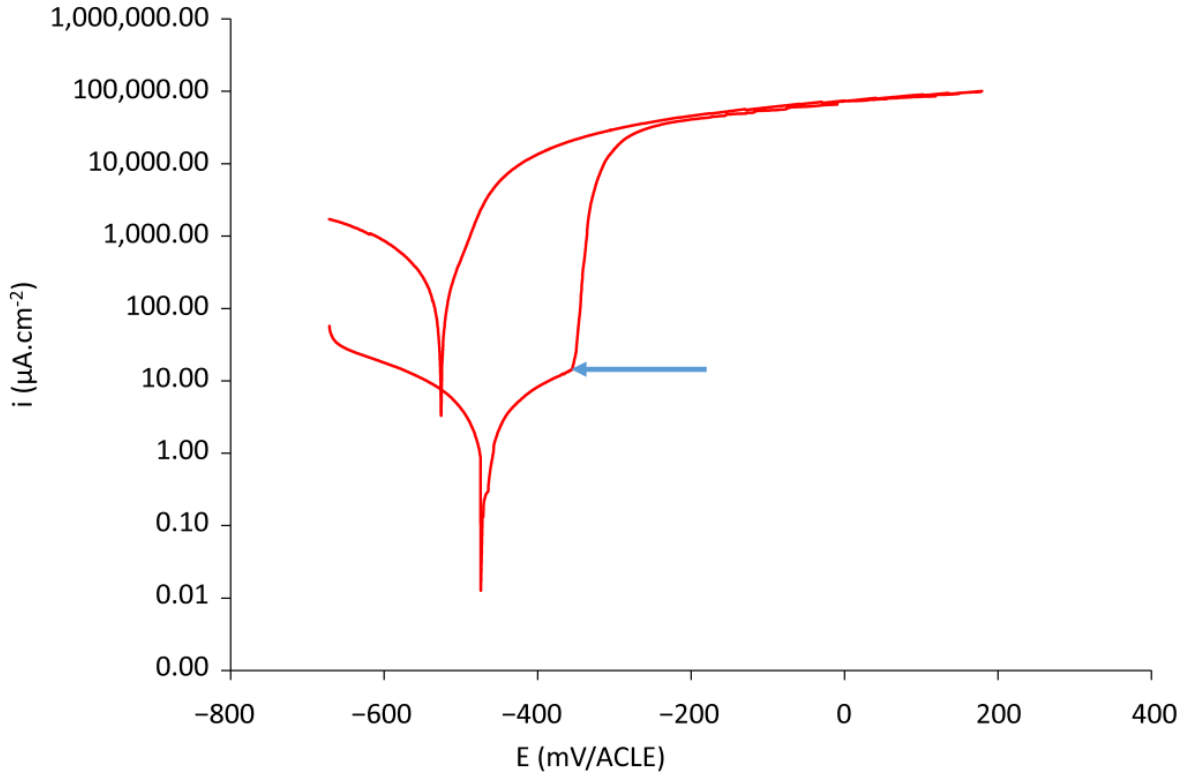

Figure 6. Potentiodynamic polarization curves of annealed experimental steel obtained in model seawater solution containing 3.5 wt.% NaCl at 70 °C with blue arrow indicating the breakdown of surface layer.

Table 3. Results of electrochemical tests of annealed experimental steel.

Heat No.	E_{corr} (mV/ACLE)	Rp ($\Omega \cdot m^2$)	i_{corr} ($\mu A \cdot cm^{-2}$)	$i_{barrier}$ ($\mu A \cdot cm^{-2}$)	$E_{barrier}$ (mV/ACLE)
T19-161	−463.4 ± 5.6	0.51 ± 0.02	0.34 ± 0.11	14.77 ± 6.21	−354.9 ± 8.6

The measured corrosion current density—i_{corr} = 0.34 μA.cm^{-2} is substantially lower than the results from potentiodynamic testing of AISI 420 martensitic stainless steel presented by Ji Sun et. al., where the authors measured i_{corr} = 6.34 μA.Cm^{-2} [14]. Another study presents an i_{corr} value of laser cladded AISI 420 at 0.117 μA.cm^{-2} [15], however the authors claim that the testing solution was injected with argon before the experiment in order to get rid of the oxygen dissolved in it, and this could lead to the lower i_{corr} values than in the other studies.

The measured i_{corr} of the experimental steel (0.34 μA.cm^{-2}) lies between the above mentioned values (from other studies [14,15]) and therefore its corrosion properties could be compared to AISI 420 (by means of the i_{corr} parameter). In comparison to other TWIP steels from other studies the E_{corr} and i_{corr} values of the tested experimental steel are considerably better than the studies of Grajcar et al. [8] and Kannan et al. [12], where their steels exhibit E_{corr} −780 and −786 mV with i_{corr} 2.0 and 22.72 μA.cm^{-2}. The main reason for the increased corrosion resistance of experimental steel lies in increased content of chromium and uniform single phase microstructure.

4. Conclusions

An experimental TWIP steel with high manganese and increased chromium content was cast and hot/cold rolled under experimental conditions. After cold rolling, this steel

was subjected to recrystallisation annealing. The samples were then laboratory tested with a focus on microstructural, mechanical and corrosion properties with the following results:

- The metal matrix of samples is single phase, fully austenitic with no presence of alpha or epsilon martensite in either the annealed or the cold rolled state.
- Microstructure after annealing is very fine-grained with an average grain size of G = 13.5 according to ASTM E112.
- The plastic deformation of this material consists of deformation twinning.
- Experimental steel reaches high strength of 976.7 $\pm$ 1.3 MPa combined with high elongation of 40.0 $\pm$ 0.5%.
- With the i_{corr} parameter, the experimental steel's corrosion resistance is similar to the martensitic stainless steel AISI 420.

Author Contributions: P.P. designed the whole experiment and chemical composition of the experimental steel; T.G. focused on testing the corrosion properties; T.S. was responsible for the sheet production and heat treatment; C.D. was the consultant for the experiment and revised the paper. All authors have read and agreed to the published version of the manuscript.

Funding: The paper was supported from ERDF Research of advanced steels with unique properties, No. CZ02.1.01/0.0/0.0/16_019/0000836.

Data Availability Statement: Not applicable.

Conflicts of Interest: The authors declare no conflict of interest.

References

1. Hofmann, H.; Mattissen, D.; Schaumann, T.W. Advanced Cold Rolled Steels for Automotive Applications. *Steel Res. Int.* **2009**, *80*, 22–28. [CrossRef]
2. Cornette, D.; Cugy, P.; Hildenbrand, A.; Bouzekri, M.; Arcelor, G.L. Ultra High Strength FeMn TWIP Steels for automotive safety parts. *Rev. Metall. Cah. D Inf. Tech. Rev. Met. Paris* **2005**, *102*, 905–918. [CrossRef]
3. De Cooman, B.C.; Estrin, Y.; Kim, S.K. Twinning-induced plasticity (TWIP) steels. *Acta Mater.* **2018**, *142*, 283–362. [CrossRef]
4. Joost, W.J. Reducing Vehicle Weight and Improving U.S. Energy Efficiency Using Integrated Computational Materials Engineering. *JOM* **2012**, *64*, 1032–1038. [CrossRef]
5. Kwon, O.; Lee, K.Y.; Kim, G.S.; Chin, K.G. New Trends in Advanced High Strength Steel Developments for Automotive Application. *Mater. Sci. Forum* **2010**, *638–642*, 136–141. [CrossRef]
6. Forejtova, L.; Kolarik, L.; Suchanek, J.; Kolarikova, M.; Pilvousek, T. Svařitelnost ocelí pro automobilové karoserie. *MM Spektrum* **2017**, *3*, 90–92.
7. Opiela, M.; Grajcar, A.; Krukiewicz, W. Corrosion behaviour of Fe-Mn-Si-Al austenitic steel in chloride solution. *J. Achiev. Mater. Manuf. Eng.* **2009**, *33*, 159–165.
8. Grajcar, A.; Kołodziej, S.; Krukiewicz, W. Corrosion resistance of high-manganese austenitic steels. *Arch. Mater. Sci. Eng.* **2010**, *41–42*, 77–84.
9. Hamada, A.S. Manufacturing, Mechanical Properties and Corrosion Behaviour of High-Mn TWIP Steels. Ph.D. Thesis, University of Oulu, Oulu, Finland, 2007.
10. Khalissi, M.; Raman, R.S.; Khoddam, S. Stress Corrosion Cracking of Novel Steel for Automotive Applications. *Procedia Eng.* **2011**, *10*, 3381–3386. [CrossRef]
11. Yuan, X.; Zhao, Y.; Li, X.; Chen, L. Effect of Cr on mechanical properties and corrosion behaviors of Fe-Mn-C-Al-Cr-N TWIP steels. *J. Mater. Sci. Technol.* **2017**, *33*, 1555–1560. [CrossRef]
12. Kannan, M.B.; Raman, R.K.S.; Khoddam, S.; Liyanaarachchi, S. Corrosion behavior of twinning-induced plasticity (TWIP) steel. *Mater. Corros.* **2013**, *64*, 231–235. [CrossRef]
13. Mujica, L.; Weber, S.; Theisen, W. Development of high-strength corrosion-resistant austenitic TWIP steel. *La Metall. Ital.* **2011**, *6*, 31–35.
14. Sun, J.; Li, J.; Xie, J.; Yang, Y.; Wu, W.; Zhou, X.; Zhang, S.; Wang, Q. Properties of rapid arc discharge plasma nitriding of AISI 420 martensitic stainless: Effect of nitriding temperatures. *J. Mater. Res. Technol.* **2022**, *19*, 4804–4814. [CrossRef]
15. Zhang, Z.; Yu, T.; Kovacevic, R. Erosion and corrosion resistance of laser cladded AISI 420 stainless steel reinforced with VC. *Appl. Surf. Sci.* **2017**, *410*, 225–240. [CrossRef]